Engineering Fracture Mechanics Vol. 13, pp. 331–347
Pergamon Press Ltd., 1980. Printed in Great Britain

ANALYSIS OF THE OPTICAL METHOD OF CAUSTICS FOR DYNAMIC CRACK PROPAGATION

ARES J. ROSAKIS
Division of Engineering, Brown University, Providence, RI 02912, U.S.A.

Abstract—In the interpretation of experimental data on dynamic crack propagation in solids obtained by means of the optical method of caustics, it has been customary to neglect the effect of material inertia on the stress distribution in the vicinity of the crack tip. In this paper, the elastodynamic crack tip stress field is used to establish the exact equations of the caustic envelope formed by the reflection of light rays from the surface of a planar solid near the tip of a propagating crack. These equations involve the instantaneous crack tip speed, the material parameters and the instantaneous dynamic stress intensity factor, and they can be used to determine the stress intensity factor for given material parameters and crack tip speed. The influence of inertial effects on stress intensity factor measurements for system parameters typical of experiments with PMMA specimens is considered. It is found that the stress intensity factor values inferred through a dynamic analysis may differ by as much as 30–40% from values based on a quasi-static analysis.

NOTATION

$$C = \frac{dvz_0}{E}$$

$C_{l,s}$ longitudinal, shear wave speeds
d thickness of specimen
D_t transverse diameter of caustic curve
E Young's modulus
$Z_p = X + iY$
$Z_p = x + iy$
K_I = mode I stress intensity factor for a stationary crack
K_{II} = mode II stress intensity factor for a stationary crack
$K_s(t)$ stress intensity factor for a running crack, evaluated using the static analysis
$K_d(t)$ stress intensity factor for a running crack, evaluated using the dynamic analysis
$K_{Id}(t)$ = mode I stress intensity factor for a running crack, evaluated using the dynamic analysis
$K_{IId}(t)$ = mode II stress intensity factor for a running crack, evaluated using the dynamic analysis

$$K'(v,t) = \left[\frac{K_d(t)\cdot(1+\alpha_s^2)\cdot(\alpha_l^2+\alpha_s^2)}{4\alpha_l\cdot\alpha_s-(1+\alpha_s^2)^2}\right]$$

$P(x,y)$ point on the actual specimen plane
$P'(X,Y)$ the image of point $P(x,y)$ on the plane of the screen
$r_l e^{i\theta_l} = x_l + y_l = x + i\alpha_l y$
$R^{(2)}$ specimen, plane
Δs optical path difference
u_z deformation of the surface of the specimen along the z direction
V_T terminal velocity of crack
$W = W_x + iW_y$, Light ray deviation vector
z_0 distance of the screen to the specimen

Greek symbols

$$\alpha_{l,s} = \left[1 - \frac{V^2}{C_{l,s}^2}\right]^{1/2}$$

$$\lambda = \frac{C}{(2\pi)^{1/2}}$$

$$\mu = C\frac{K'(V,t)}{(2\pi)^{1/2}}$$

ν = Poisson's ratio

$$\xi = \left[\frac{2\alpha_s}{1+\alpha_s^2}\cdot\frac{K_{IId}(t)}{K_{Id}(t)}\right]$$

$\rho_0 = (\frac{3}{2}\mu\alpha_l)^{2/5}$ radius of the approximated initial curve in the (x_l, y_l) plane.
$\sigma_{1,2}$ principal stresses at a point

$$\phi = \tan^{-1}\frac{K_{II}}{K_I}$$

$\phi' = \tan^{-1}\xi$
ω^- region inside the initial curve
ω^+ region outside the initial curve
Ω^- region inside the caustic
Ω^+ region outside the caustic

INTRODUCTION

AN OPTICAL method has been developed [1, 2–5] for the study of the stress singularity in the vicinity of a crack tip under conditions of plane stress. The method, known as the method of "caustics", has been extensively applied for the analysis of stress fields near the tip of stationary cracks [2–4]. Recently Kalthoff *et al.* [9, 10] and Theocaris *et al.* [6–8] presented work using the method of caustics for the study of propagating cracks. So far the method has been used under the basic assumption of a static solution for the stress–strain field near the crack tip. When dealing, however, with propagating cracks, an exact solution would require the introduction of the dynamic stress–strain distribution ahead of the crack tip, as well as the use of the dynamic elastic moduli E, ν, for cases of dynamic loading conditions.

Theocaris was the first to measure and use the dynamic moduli [7, 8, 11], instead of the static ones, for the interpretation of caustic envelopes in cases of dynamic loading. The next step was that of Kalthoff *et al.* [9] who very recently introduced a correction factor to account for the error made by using the static analysis in cases of propagating cracks. The correction factor was obtained by using a series of simplifying assumptions based on numerical calculations.

In this paper the equations of the caustic envelope are obtained in a very simple form. Some approximations, based on analytical considerations are introduced without resorting to numerical arguments. A generalization of the results to include both opening and sliding mode propagating cracks is made in the Appendix.

1. CAUSTICS BY REFLECTION

An incident beam of parallel light rays is reflected from the near crack tip region of the specimen. Because of non-uniform contraction of the specimen in the thickness direction, the reflected rays deviate from parallelism and, under suitable conditions, generate a three-dimensional surface in space which separates an illuminated region from a dark region (see Fig. 1). That surface, composed of points of maximum luminosity or thermal effect, is called the "caustic" surface (Greek καυστικός, burning). The rays are tangent to the caustic surface, and the cross-sections of the surface can be observed as bright curves on a screen parallel to the specimen.

Let $u_z = u_z(x, y)$ be the normal displacement of the surface of the specimen due to the stresses at the vicinity of the crack tip. Consider a parallel beam of light illuminating the surface. If a screen is placed at a distance z_0 from the mid-surface of the specimen, a light ray impinging on point $P(x, y)$, will be reflected and recorded on the screen, giving an image point $P'(X, Y)$.

The deviation $W = W_x + iW_y$ of P' from the projection of P on the screen, will depend on the angle of reflection and on z_0. W will be a function of the slopes $\frac{\partial u_z}{\partial x}, \frac{\partial u_z}{\partial y}$ of the deformation surface, and of the distance z_0 of the screen to the specimen (see Fig. 2).

It has been shown [5] that

$$W = 2z_0 \operatorname{grad}_{x,y}[u_z(x, y)] \Rightarrow Z_{p'} = J_p + W = J_p + z_0 \operatorname{grad}_{x,y}[2u_z(x, y)] \tag{1.1}$$

where $J_p = x + iy$ and $Z_{p'} = X + iY$. The quantity $2u_z(x, y) = \Delta S(x, y)$ represents the extra distance traveled by the ray because of the lateral deformation of the vicinity of the crack tip. ΔS is called the optical path difference.

Equation (1.1) is the governing equation of the mapping of points $P(x, y)$ of the specimen on to points $P'(X, Y)$ on the screen.

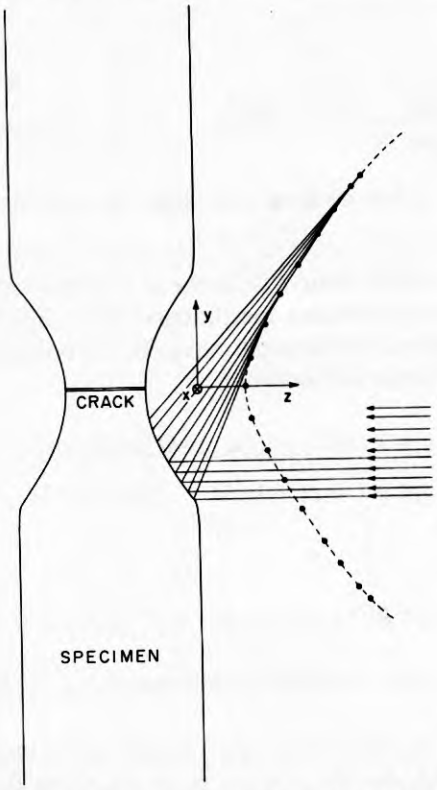

Fig. 1. Three dimensional caustic envelope formed by reflection (not in scale).

What appears on the screen is a completely dark area around the crack tip, surrounded by a bright region. The boundary between the bright and the dark regions is a highly luminous curve, the caustic curve. Equation (1.1) is a definite relation connecting points on the (X, Y) plane of the screen to generic points on the specimen plane (x, y). Experiment implies that there is a region in the (X, Y) plane on which no point of the (x, y) plane is mapped (shadow region). The whole (x, y) plane will therefore map in only part of the (X, Y) plane.

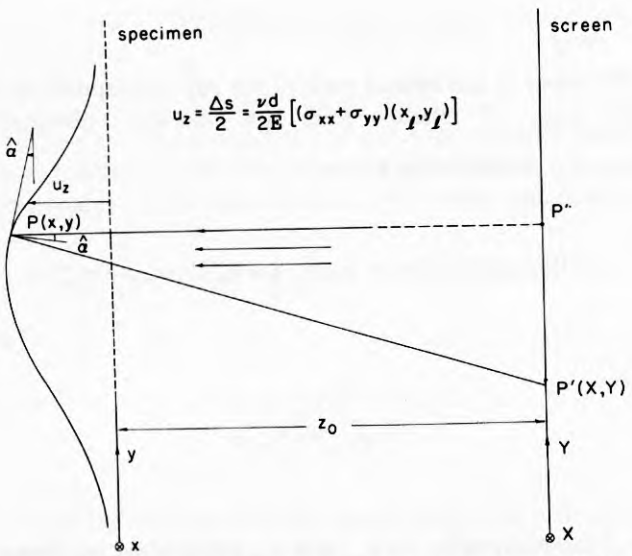

Fig. 2. The mapping of points $P(x, y)$ of the specimen, to points $P'(X, Y)$ on the screen.

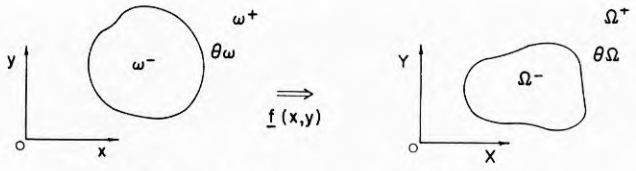

Fig. 3. Left: the initial curve; Right: the caustic curve.

It has been shown that there is a curve $\partial\omega$ in the (x, y) plane with the following properties: (i) every point outside $\partial\omega$ maps outside a specific curve $\partial\Omega$ in the (X, Y) plane. (ii) every point inside $\partial\omega$, maps again outside or on the same curve $\partial\Omega$. (iii) points on $\partial\omega$ will map on $\partial\Omega$ (see Fig. 3) or in standard mathematical notation:

$$\forall(x,y)\in\omega^{-}\upsilon\omega^{+}\Rightarrow \underline{f}(x,y)\in\Omega^{+}\upsilon\partial\Omega$$

$$\forall(x,y)\in\partial\omega\Rightarrow \underline{f}(\partial\omega)\underline{\subseteq}\partial\Omega \qquad \text{(see Fig. 3)}$$

or equivalently:

$$\nexists(x,y)\in R^{(2)}\ni \underline{f}(x,y)\in\Omega^{-}\Rightarrow f^{-1}(\Omega^{-})=\emptyset.$$

The above statements imply that there are no points in the (x, y) plane (of the specimen) that are mapped into region Ω^{-}.

One can identify the Ω^{-} as the shadow region and Ω^{+} as the bright one. The boundary $\partial\Omega$ between the bright and the shadow regions is, as we know from experiment, a highly luminous curve, the "caustic". High luminosity implies multiple mapping coming from both $\partial\omega$ and ω^{-}, and therefore the Jacobian of the transformation of points (x, y) on the specimen on to points (X, Y) on the image plane must vanish there. The condition $J=\dfrac{\partial(X,Y)}{\partial(x,y)}=0$ provides the *locus* of points $\partial\omega$ which correspond to the luminous curve where multiple mapping occurs. $\partial\omega$ is called the "initial curve".

2. THE CAUSTIC CURVE OBTAINED BY A DYNAMIC FIELD AT THE VICINITY OF A PROPAGATING CRACK TIP

As we have seen in the previous section, the deviation from parallelism of a reflected light ray at a distance z_0 from the middle surface of the specimen, can be expressed by:

$$W = z_0\,\mathrm{grad}_{x,y}\,[\Delta S(x,y)]$$

where ΔS is the difference in the optical path of the ray corresponding to a generic point $P(x, y)$. For the case of plane stress for caustics obtained by reflection, $\Delta S = 2u_z = \dfrac{\mathrm{d}\nu}{E}(\sigma_1+\sigma_2)$. Substituting above:

$$W = z_0\underline{\nabla}_{x,y}\left[(\sigma_1+\sigma_2)\frac{\mathrm{d}\nu}{E}\right] = C\underline{\nabla}_{x,y}(\sigma_{xx}+\sigma_{yy}) \tag{2.1}$$

where

$$C=\frac{\mathrm{d}\nu z_0}{E}.$$

Making use now of the expression for σ_{xx} and σ_{yy} established by Freund [12–14] which represent the stress components in the vicinity of the tip of a crack propagating with variable

velocity $V(t)$, we have:

$$\sigma_{xx} = \frac{K_d(t)}{\sqrt{2\pi}} \cdot B_1(V)\left[(1 + 2\alpha_l^2 - \alpha_s^2)\frac{\cos(\theta_l/2)}{r_l^{1/2}} - \frac{4\alpha_l\alpha_s}{(1+\alpha_s^2)}\frac{\cos(\theta_s/2)}{r_s^{1/2}}\right] \tag{2.2}$$

$$\sigma_{yy} = \frac{K_d(t)}{\sqrt{2\pi}} \cdot B_1(V)\left[-(1 + \alpha_s^2)\frac{\cos(\theta_l/2)}{r_l^{1/2}} + \frac{4\alpha_l\alpha_s}{(1+\alpha_s^2)}\frac{\cos(\theta_s/2)}{r_s^{1/2}}\right] \tag{2.3}$$

where:

$$r_l e^{i\theta_l} = x_l + iy_l = x + i\alpha_l y$$

$$\alpha_l = \left[1 - \frac{V^2}{C_l^2}\right]^{1/2}, \qquad \alpha_s = \left[1 - \frac{V^2}{C_s^2}\right]^{1/2}.$$

$$B_1(V) = \frac{(1+\alpha_s^2)}{[4\alpha_l\alpha_s - (1+\alpha_s^2)^2]}$$

subscripts l and s referring to the longitudinal and shear way speeds, C_l and C_s, in the specimen material. It is worth noting that the above expressions were derived under the assumptions of elastic fracture behavior with V representing the instantaneous crack tip speed for non-uniform rates of crack growth. Adding (2.2) and (2.3) we obtain:

$$\sigma_{xx} + \sigma_{yy} = \frac{K_d(t)B_1(V)}{\sqrt{2\pi}}(2\alpha_l^2 - 2\alpha_s^2)\frac{\cos(\theta_l/2)}{r_l^{1/2}}$$

$$= \left[\frac{K_d(t)(1+\alpha_s^2)(\alpha_l^2 - \alpha_s^2)}{[4\alpha_l\alpha_s - (1+\alpha_s^2)^2]}\right] \cdot \sqrt{\frac{2}{\pi r_l}} \cdot \cos(\theta_l/2)$$

$$= K'(V,t) \cdot \sqrt{\frac{2}{\pi r_l}} \cdot \cos(\theta_l/2) \tag{2.4}$$

where $r_l e^{i\theta_l} = x_l + iy_l = x + i\alpha_l y$. Equation (2.4) gives the dynamic stress field $\sigma_{xx} + \sigma_{yy}$ at each point (x, y) as a function of the parameters (x_l, y_l) where $x_l = x$, $y_l = \alpha_l y$. It is worth observing that the dynamic expression (2.4) is of the same functional form as the static formula, $\sigma_{xx} + \sigma_{yy} = K_{st}\sqrt{\frac{2}{\pi r}}\cos(\theta/2)$ with two main differences: first, the existence of a multiplying factor

$$\frac{(1+\alpha_s^2)(\alpha_l^2 - \alpha_s^2)}{4\alpha_l\alpha_s - (1+\alpha_s^2)^2}$$

and second, the fact that the dynamic field has been scaled in the y direction only, by a factor α_l. One should note that (2.4) which gives the $\sigma_{xx} + \sigma_{yy}$ for a running crack reduces to the stationary for $V = 0$.

(i) *The Equations of the mapping*

For the case of a propagating crack the deviation W corresponding to the generic point (x, y) is given by:

$$W = C\nabla_{x,y}[(\sigma_{xx} + \sigma_{yy})(x_l, y_l)]$$

$$\Rightarrow W = C\frac{\partial}{\partial x_l}[(\sigma_{xx} + \sigma_{yy})(x_l, y_l)]\frac{\partial x_l}{\partial x} + iC\frac{\partial}{\partial y_l}[(\sigma_{xx} + \sigma_{yy})(x_l, y_l)]\frac{\partial y_l}{\partial y}$$

$$\Rightarrow W = C\frac{\partial}{\partial x_l}[(\sigma_{xx} + \sigma_{yy})(x_l, y_l)] + iC\frac{\partial}{\partial y_l}[(\sigma_{xx} + \sigma_{yy})(x_l, y_l)]\alpha_l.$$

The image $P'(X, Y)$ on the screen of the point $p(x, y)$ of the specimen will be given by:

$$\left.\begin{aligned} X &= x + C\frac{\partial}{\partial x_l}[(\sigma_{xx} + \sigma_{yy})(x_l, y_l)] \\ Y &= y + \alpha_l C\frac{\partial}{\partial y_l}[(\sigma_{xx} + \sigma_{yy})(x_l, y_l)] \end{aligned}\right\} \tag{2.5}$$

using now eqn (2.4) for the stresses and the fact that $x = r_l\cos\theta_l$ and $y = \dfrac{r_l\sin\theta_l}{\alpha_l}$, we get:

$$\left.\begin{aligned} X &= r_l\cos\theta_l + \mu r_r^{-3/2}\cos\frac{3\theta_l}{2} \\ Y &= \frac{r_l\sin\theta_l}{\alpha_l} + \alpha_l\mu r_r^{-3/2}\sin\frac{3\theta_l}{2} \end{aligned}\right\} \tag{2.6}$$

where

$$\mu = C\frac{K'(V, t)}{(2\pi)^{1/2}}, \qquad 0 < \theta_l < 4\pi.$$

Equations (2.6) are the governing equations for the mapping of a generic point $P(x, y)$ of the specimen on to a point $P'(X, Y)$ of the screen. They are expressed with respect to the parameters (r_l, θ_l) which are connected to (x, y) by the relation $r_l e^{i\theta_l} = x + i\alpha_l y = x_l + iy_l$. It will become obvious from the following that by using (r_l, θ_l) as the parameters instead of (r, θ), the equations of the caustic will result in a very convenient form to work with.

It is worth noting that points $P(x, y)$ lying on a member of the family of ellipses $x^2 + \alpha_l^2 y^2 = \rho^2$ on the (x, y) plane, map on to points on the parameter plane (x_l, y_l) lying on the circle $x_l^2 + y_l^2 = \rho^2 = r_l^2$. Those points will in turn map through the transformation eqn (2.6) on to points $P'(X, Y)$ lying on the curve:

$$\left.\begin{aligned} X &= \rho\cos\theta_l + \mu\rho^{-3/2}\cos\frac{3\theta_l}{2} \\ Y &= \rho\frac{\sin\theta_l}{\alpha_l} + \alpha_l\mu\rho^{-3/2}\sin\frac{3\theta_l}{2} \end{aligned}\right\} \qquad 0 < \theta_l \leq 4\pi. \tag{2.7}$$

Thus a member of the family of ellipses $x^2 + \alpha_l^2 y^2 = \rho^2$ defined on the actual plane of the specimen, will map on a member of the family of curves (2.7) defined on the plane of the specimen.

(ii) *The equations of the caustic*

The condition for the existence of a caustic curve surrounding the shadow region is the vanishing of the Jacobian of the transformation [3]. The condition $J = \dfrac{\partial(X, Y)}{\partial(x, y)} = 0$ in general will give a curve on the (x, y) plane. Points both inside and outside this curve will

always map on or outside the caustic envelope. Points on this curve will map upon the caustic envelope. The curve obtained by setting $J = 0$, lying on the (x, y) plane is called the "*initial curve*".

$$J = \frac{\partial(X, Y)}{\partial(x, y)} = \alpha_l \frac{\partial(X, Y)}{\partial(x_l, y_l)} = 0 \Rightarrow \frac{\partial(X, Y)}{\partial(x_l, y_l)} = 0.$$

Using now eqn (2.6) and the polar form of the Jacobian we get:

$$\Rightarrow \frac{\partial(X[r_l, \theta_l] Y[r_l, \theta_l])}{\partial(r_l, \theta_l)} = 0$$

$$\Rightarrow \boxed{r_l^5 - \tfrac{9}{4}\mu^2\alpha_l^2 + \tfrac{3}{2}\mu r_l^{5/2}(\alpha_l^2 - 1)\cos\frac{5\theta_l}{2} = 0} \quad . \tag{2.8}$$

Since we have chosen to work with (r_l, θ_l) as parameters instead of the actual coordinates (r, θ), the condition $J = 0$ gives a curve with respect to (r_l, θ_l), which is the equation of the image of the "*initial curve*" in the (r_l, θ_l) plane. Equation (2.8) gives the region in the (r_l, θ_l) plane whose points map on to the caustic curve.

The *exact* equations of the caustic envelope are therefore given by:

$$\left.\begin{aligned} X &= r_l \cos\theta_l + \mu r_l^{-3/2} \cos\frac{3\theta_l}{2} \\ Y &= \frac{1}{\alpha_l}\left[r_l \sin\theta_l + \alpha_l^2 \mu r_l^{-3/2} \sin\frac{3\theta_l}{2} \right] \end{aligned}\right\} \tag{2.9}$$

under the constraint:

$$r_l^5 - \tfrac{9}{4}\mu^2\alpha_l^2 + \tfrac{3}{2}\mu r_l^{5/2}(\alpha_l^2 - 1)\cos\frac{5\theta_l}{2} = 0.$$

The curve described by eqn (2.8) has a very weak θ_l dependence, especially for low or medium values of V. Although the analytic expressions presented above are not unduly cumbersome, it is advantageous nonetheless to simplify them somewhat in order not to have to resort to numerical schemes. As it turns out, a very close approximation can be made regardless of the value of α_l.

The method of approximation adopted here is to find a set of circles each of which constitutes a best fit to (2.8) for each value of α_l. The procedure for finding the best fit circles is as follows: As shown above, a family of circles, on the (r_l, θ_l) plane, map on to a family of image curves given by eqn (2.6) (for different r_l) lying in the (X, Y) plane.

The circle which gives the closest fit to the curve represented by eqn (2.8), will be the one corresponding to that particular member of the (2.6) image family with the smallest enclosed area. This can be demonstrated as follows:

Let $r_l = \rho_0$ be the radius of the circle corresponding to the minimum area member of the (2.6) family (see Fig. 4). Let the dotted curve in the (x_l, y_l) plane correspond to curve (2.8), and the dotted curve in the (X, Y) plane to its image. Any point on $r_l = \rho_0$, whether inside or outside the dotted curve (2.8), will map outside the dotted image curve in the (X, Y) plane, except at those points where the curves touch (solid line).

Since the circle $r_l = \rho_0$ by hypothesis maps on to the minimum area member of the (2.6) family, every circle of smaller or larger radius than ρ_0 will map on to a member of the (2.6) family having a greater area than the curve corresponding to $r_l = \rho_0$. Consequently, the image of any other circle will lie further away from the dotted curve than the image of $r_l = \rho_0$

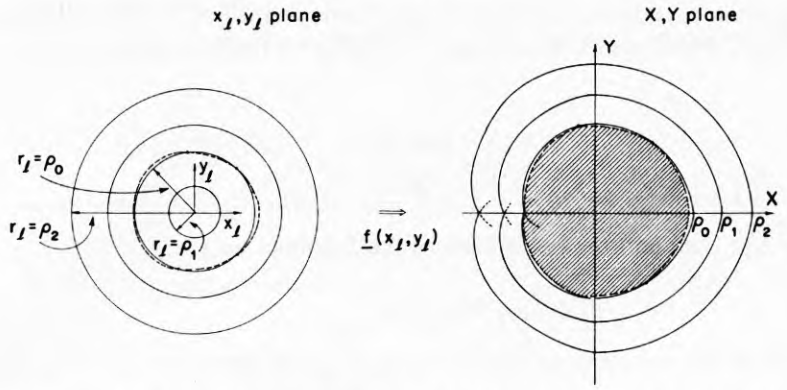

Fig. 4. Left: the image of the initial curve on the (x_l, y_l) plane (dotted), and its best circle approximation; Right: the caustic (dotted) and its best approximation curve.

does. The dotted curve in the (X, Y) plane is the caustic, and $r_l = \rho_0$ is the closest circle approximation to the (2.8) curve, since it gives an image which is the closest curve possible to the caustic.

3. EVALUATION OF ρ_0

In order to find ρ_0 let us consider the area of a random member of the family of images:

$$E = \frac{1}{2}\int_0^{4\pi} (XY'_{\theta_l} - YX'_{\theta_l})\,\mathrm{d}\theta_l.$$

Substituting the expressions for $X, X'_{\theta_l}, Y, Y'_{\theta_l}$ from (2.4) we get:

$$E = \frac{1}{2}\frac{4\pi}{\alpha_l}[r_l^2 + \tfrac{3}{2}\mu^2\alpha_l r_l^{-3}].$$

The condition for an extremum gives:

$$\left.\frac{\partial E}{\partial r_l}\right|_{r_l=\rho 0} = 0 \Rightarrow \rho_0 = (\tfrac{3}{2}\mu\alpha_l)^{2/5} \tag{3.1}$$

which corresponds to a minimum, since $\left.\dfrac{\partial E^2}{\partial^2 r_l}\right|_{r_l=\rho 0} > 0$. Thus $r_l = \rho_0$ gives the minimum area member of the image (2.6) family.

Using the results of the above section, we conclude that $r_l = \rho_0 = (\frac{3}{2}\mu a_l)^{2/5}$ corresponds to the closest circle approximation to the curve represented by eqn (2.8). To find where the circle and the (2.8) curve touch, one can solve equations $r_l = \rho_0$ and eqn (2.8) simultaneously. One can thus see that the two curves touch at a total of 5 points. The coordinates of these 5 points in the (r_l, θ_l) plane are given by $r_l = \rho_0$ and by: $\cos\dfrac{5\theta_l}{2} = 0$. The latter provides 5 values of θ_l, namely, $\theta_l = \dfrac{\pi}{5}, \dfrac{3\pi}{5}, \pi, \dfrac{7\pi}{5}, \dfrac{9\pi}{5}$.

Since $r_l = \rho_0$ and the curve represented by eqn (2.8) touch in 5 points, their corresponding images in the (X, Y) plane will touch in 5 points as well.

4. (i) BEST APPROXIMATION OF THE INITIAL CURVE

Up to this point we have almost totally worked in the (r_l, θ_l) plane, investigating the best circle estimate to the (2.8) curve.

As we have seen above, the (2.8) curve is just the image of the initial curve on the parametric plane (x_l, y_l) and it has no physical meaning. Although it is easier to work in the

(r_l, θ_l) plane, it is instructive to investigate which is the best fit curve to the initial curve in the actual (x, y) specimen plane.

As shown above, the equation of the best circle approximation to the (2.8) curve (image of the initial curve in the (x_l, y_l) plane) is given by $r_l^2 = \rho_0^2 = x_l^2 + y_l^2 = (\frac{3}{2}\mu\alpha_l)^{4/5}$. In the actual (x, y) plane, the corresponding points (r, θ) lie on the ellipse $x^2 + \alpha_l^2 y^2 = (\frac{3}{2}\mu\alpha_l)^{4/5}$, since $x_l = x$, $y_l = \alpha_l y$. This ellipse is therefore the best approximation of the initial curve.

Thus we have seen that the initial curve in the (x, y) (specimen plane) for a propagating crack can be approximated by the ellipse:

$$\boxed{x^2 + \alpha_l^2 y^2 = (\tfrac{3}{2}\mu\alpha_l)^{4/5}} \qquad \text{for all values of } v \text{ and } \alpha_l, \alpha_s \tag{4.1}$$

which reduces to:

$$x^2 + \alpha_l^2 y^2 = \left[\frac{3}{2}\left(\frac{(1+\alpha_s^2)(\alpha_l^2 - \alpha_s^2)}{4\alpha_l\alpha_s - (1+\alpha_s^2)^2}\right) \cdot \alpha_l \frac{K_d(t)\, dv z_0}{E(2\pi)^{1/2}}\right]^{4/5}$$

when the values of μ and C are substituted in (4.1).

(ii) *The behavior of the approximation curve as* $V \to 0$

As a check to the approximation curve (4.1) one could examine its behavior as $V \to 0, \alpha_l, \alpha_s \to 1$. Taking the limit as $\alpha_s, \alpha_l \to 1$, eqn (4.1) reduces to:

$$x^2 + y^2 = \left[\frac{3}{2}\frac{v}{E}\frac{dz_0 K_d(t)}{(2\pi)^{1/2}}\right]^{4/5} = \rho_{st}^2$$

which is the known equation of the initial curve obtained by using the stress field of a stationary crack [4]. Thus our approximation curve (4.1) reduced to the exact equation of the initial curve as $V \to 0$.

5. (i) THE APPROXIMATE EQUATIONS OF THE CAUSTIC CURVE

After the approximation is made, the eqn (2.9) of the caustic become:

$$\left.\begin{aligned} X &= r_l \cos\theta_l + \mu r_l^{-3/2} \cos\frac{3\theta_l}{2} \\ Y &= \frac{1}{\alpha_l}\left[r_l \sin\theta_l + \alpha_l^2 \mu r_l^{-3/2} \sin\frac{3\theta_l}{2}\right] \end{aligned}\right\} \tag{5.1}$$

where

$$r_l = \rho_0 = (\tfrac{3}{2}\alpha_l\mu)^{2/5}.$$

Equations (5.1) can be expressed as follows:

$$\left.\begin{aligned} X &= \rho_0\left[\cos\theta_l + \tfrac{2}{3}\alpha_l^{-1}\cos\frac{3\theta_l}{2}\right] \\ Y &= \frac{\rho_0}{\alpha_l}\left[\sin\theta_l + \tfrac{2}{3}\alpha_l \sin\frac{3\theta_l}{2}\right] \end{aligned}\right\} \tag{5.2}$$

where

$$0 < \theta_l \leq 4\pi.$$

Equations (5.2) are the parametric equations of the caustic curve. As $V \to 0, \alpha_l, \alpha_s \to 1, \rho_0 \to \rho_{st}$ the above equations become the equations of a generalized epicycloid as predicted by the analysis of stationary cracks.

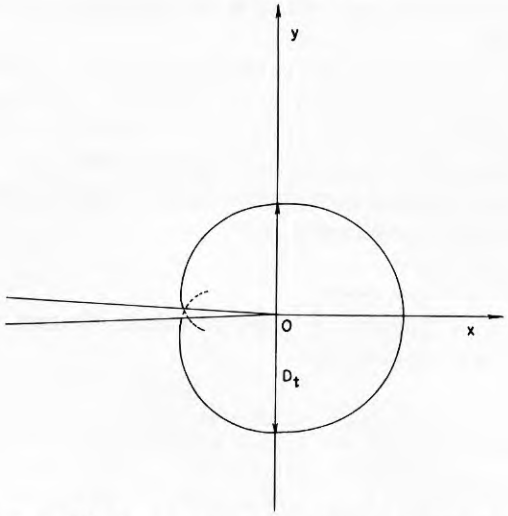

Fig. 5. Evaluation of the dynamic stress intensity factor $K_d(t)$ by measurement of D_t.

The parameter ρ_0 of the eqn (5.2) is a function of the elastic moduli E and ν. For propagating cracks under dynamic loading conditions, the dynamic values of the moduli E and ν must be calculated and used for the evaluation of ρ_0, as suggested by Theocaris *et al.* [7, 8, 11].

(ii) *Evaluation of* $K_d(t)$

By employing eqn (5.2) the geometric properties of the curve can be investigated (see Fig. 5). The transverse diameter D_t of the curve can be evaluated with respect to $K_d(t)$ at a given value of α_l. By setting $X = 0$ one obtains values of θ_l and hence values of the Y intercepts and D_t with respect to $K_d(t)$. Hence by measuring D_t, the stress intensity factor can be calculated.

(iii) *Concluding remarks*

Expressing the equations of the caustic envelope with respect to the parametric (r_l, θ_l) plane, one obtains more convenient and shorter forms than one would do expressing them with respect to the (r, θ) physical plane of the specimen.

The resulting equations are simplified further by using the approximation scheme described above. The approximations lead to an elliptical initial curve in the (r, θ) plane. This does not contradict intuition. It is known that for the cases of propagating cracks the $\sigma_{xx} + \sigma_{yy}$ stress field is scaled in the y direction, thus deforming the circular initial curve, corresponding to a static crack, to an ellipse as the velocity becomes finite.

The resulting equations are not limited to a certain range of velocities since the approximation curves depend each time on α_l and α_s. The method is therefore quite a general one, without the generality implying complications in the resulting equations. The simple form of the equations together with the lack of restrictions in the range of v justifies the use of the corrected formulae for cases of propagating cracks.

6. (i) CORRECTION DUE TO DYNAMIC EFFECTS

It is very instructive to calculate the error introduced in the evaluation of the dynamic stress intensity factor by using the static equations of the caustic curve, instead of the dynamic ones. Such a calculation will show if the use of the static analysis gives accurate enough results, and, if so, in which range of crack velocities.

For calculating the error, eqns (5.2) were used to evaluate the dynamic stress intensity factor for different velocities of a crack at a given material. The ratio of the calculated values over the ones corresponding to the same velocity, and obtained by the static analysis, were subsequently plotted against the velocity of the propagating crack.

The material for which the calculations were performed was PMMA (polymethyl-methacrylate). PMMA was chosen since it behaves in close approximation to an ideally

brittle material, that is, its behavior is well described by linear elastic fracture mechanics.

In addition to the above, PMMA has been used by a considerable number of investigators and therefore large numbers of experimental data are available in the literature concerning its material properties and fracture behavior (elastic moduli, limiting crack velocities, etc.).

The material parameters for PMMA in cases of experiments performed under conditions of low loading rates were taken to be the following:

$$\rho = 1200\,\mathrm{kg\,m^{-3}} \qquad \text{Density}$$

$$\nu = 0.34 \qquad \text{Poisson's ratio}$$

$$E = 3200\,\mathrm{MN\,m^{-2}} \qquad \text{Young's modulus}$$

for which the values of the shear and longitudinal wave speeds were found to be equal to:

$$C_l = 2025\,\mathrm{m\,s^{-1}} \qquad \text{Longitudinal wave speed}$$

$$C_s = 997.5\,\mathrm{m\,s^{-1}} \qquad \text{Shear wave speed.}$$

The ratio $\dfrac{K_d(t)}{K_{st}(t)}$ was plotted v crack velocity (see Fig. 6i, ii).

(ii) *The error*

It can be seen from Fig. 6(i) that for low values of velocities, ranging between (0–200) $\mathrm{m\,s^{-1}}$, the error is small, lying between 0% to 2.0%. For medium velocities in the range of (250–350) $\mathrm{m\,s^{-1}}$ it becomes significantly large, lying between 3.2 and 6.2%.

Finally, for velocities in the range of 400–700 $\mathrm{m\,s^{-1}}$ (the terminal velocity of cracks in PMMA), the error becomes very large, ranging from 8.4 to 45.6%.

The range of velocities considered in Fig. 6(i) was dictated by a theoretical estimate of the maximum terminal velocity of Mode I cracks in PMMA. The theoretical estimate of the terminal velocity was in agreement with experimental results obtained by a number of investigators.

(iii) *The terminal velocity*

A number of attempts, based on energy arguments, have been made to predict the maximum velocity of cracks propagating in brittle materials. In 1972 Bergvist [15] using the experimental results of Paxson and Lucas [16] for PMMA, arrived at an approximate expression for the terminal velocity in PMMA which was given by:

$$V_T = 0.69C_s = 0.42\left(\frac{E}{\rho}\right)^{1/2}. \tag{6.3}$$

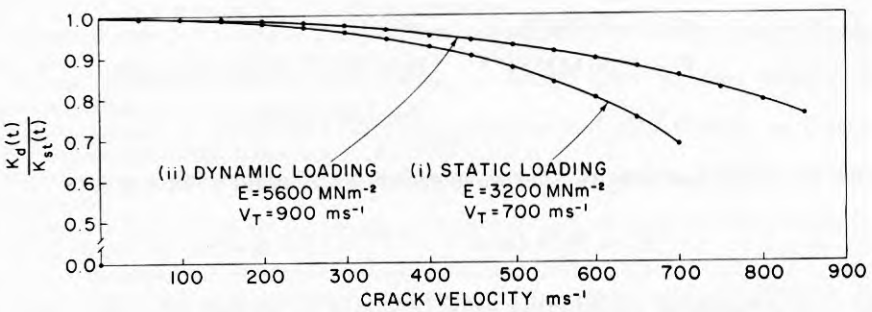

Fig. 6. The ratio $\dfrac{K_d(t)}{K_{st}(t)}$ v crack velocity in PMMA.

From (6.3) one can get a value for the maximum terminal velocity of the crack in PMMA. In our case the estimated velocity was found to be $686\,\mathrm{m\,s^{-1}}$. The highest velocities in PMMA reported in the literature do not deviate much from this value. Schardin [17] reported the value of $655\,\mathrm{m\,s^{-1}}$, Dulaney and Brace [18], $670\,\mathrm{m\,s^{-1}}$, Cotterel [19] $670\,\mathrm{m\,s^{-1}}$, Theocaris *et al.* [22] $670\,\mathrm{m\,s^{-1}}$ and Dahlberg [20] $700\,\mathrm{m\,s^{-1}}$.

From the above one can see that for PMMA under conditions of static loading (low loading rates), the range of possible crack velocities is between $0\,\mathrm{m\,s^{-1}}$ and $700\,\mathrm{m\,s^{-1}}$. The above estimated upper limit of crack tip velocities in PMMA, combined with the results of Fig. 6, show that there is a substantial range of velocities, between $350\,\mathrm{m\,s^{-1}}$ and $700\,\mathrm{m\,s^{-1}}$ corresponding to an error between 6.5 and 45.6%.

(ii) *Dynamic loading rates*

The results obtained above hold for cases of experiments performed under static loading conditions (low loading rates). Since PMMA is a viscoelastic material, the elastic moduli increase considerably at very high loading rates. To describe therefore the fracture behavior of PMMA for cases of high loading rates, one requires the knowledge of the elastic parameters corresponding to the loading rates used. In experimental investigations of the dynamic behavior of solids, a large number of devices have been used. These range from direct modification of conventional testing machines, resulting in higher rates of loading, to the use of impact testing, ultrasonic or high explosive techniques.

For cases of explosive loading, the dynamic value of Young's modulus was found to be almost double its static value. From experiments performed by Davies *et al.* [21] in PMMA, it was shown that the dynamic Young's modulus can reach a value as high as $6000\,\mathrm{MN\,m^{-2}}$. The above value was obtained from experiments performed using a split Hopkinson bar, the specimen being loaded explosively. The compressive loading cycles were of $30\,\mu\mathrm{s}$ duration.

In relation to the method of caustics, Theocaris *et al.* calculated the dynamic values of the Young's modulus and Poisson's ratio by comparing the sizes of the caustics formed at the tips of stationary notches in PMMA under conditions of static or dynamic loading. His experiments showed that for loading rates of $0.35\,\mathrm{s^{-1}}$, the Poisson's ratio of the material remained the same, whereas the Young's modulus increased to a value of $E = 4300\,\mathrm{Nm^2}$ [22]. He was the first to measure and introduce the dynamic moduli in the equations of the caustics used for the study of running cracks under conditions of impact loading [11].

Since the Young's modulus increases under conditions of dynamic loading, the Poisson's ratio remaining constant, the wave speeds must increase as well, resulting in a higher terminal velocity of the propagating crack. The error in cases of very high loading rates (higher values of $C_{l,s}$, lower values of $\alpha_{l,s}$) is expected to be less pronounced for small or moderate values of velocity, than the equivalent error obtained for cases of static loading. The range of obtainable velocities, however, will be increased (V_T going up with loading rate), still giving a considerable error at high velocities. To investigate the effect of loading rate on the difference between the static and dynamic analysis, values of $\dfrac{K_d(t)}{K_{st}(t)}$ were plotted vs crack tip velocity for case of experiments performed under conditions of impact loading. See Fig. 6(ii). The dynamic values of the parameters used were as follows:

$\rho = 1200\,\mathrm{Kg\,m^{-3}}$	Density
$E = 5600\,\mathrm{MN\,m^{-2}}$	Dynamic Young's modulus
$\nu = 0.34$	Poisson's ratio

for which the shear and longitudinal wave speeds were found to be equal to

$$C_l = 2678.4\,\mathrm{m\,s^{-1}} \qquad C_s = 1319\,\mathrm{m\,s^{-1}}.$$

For the case considered, the limiting velocity would be around $900\,\mathrm{m\,s^{-1}}$. This value is verified by the experiments performed by Theocaris [11] who reported velocities up to $850\,\mathrm{m\,s^{-1}}$.

(iii) *The error in cases of impact loading*

From comparison between curves (i)–(ii) in Fig. 6 one can see that the error is more pronounced for cases of low loading rates than for cases of higher rates. Figure 6(ii) shows that for low values of the crack velocity ranging between (0–250) m s^{-1}, the error is negligible, lying between 0 and 1.5%.

For medium velocities in the range of (300–500 m s^{-1}) it is small, ranging between 2 and 7.8%. Finally, for velocities in the range of 550–900 m s^{-1} (the terminal velocity for impact loading rates), the error becomes considerably larger, ranging from 9.6 to 38.0%.

7. THE EXACT EQUATIONS

The calculations described in the foregoing section were repeated using the exact dynamic equations of the caustic curve, given in (2.9). An IBM 360 computer was employed for the calculation. The results obtained were almost exactly coincident with the values shown in Fig. 6(i) and (ii). The values of $\frac{K_d(t)}{K_{st}(t)}$ were found to differ by less than 0.002 for every value of V.

The agreement in the results of the two cases is very close, indicating that the theoretically obtained approximation to eqn (2.9), described in Section 2(ii), is indeed justifiable.

CONCLUSIONS AND SUMMARY

The exact equations of the caustic curve for the case of a running crack were obtained in a simple form with respect to the (r_l, θ_l) parametric plane. These were further simplified by employing a theoretical argument. The error introduced by using the static analysis was then calculated by making use of *both* the exact and simplified dynamic formulae.

The numerical results obtained showed that the use of the approximate dynamic formulae is indeed justifiable. At the same time, it was shown that there is a considerably large range of velocities lying between $V_T/2$ and V_T corresponding to errors between 6.5 and 45.6%.

Acknowledgements—In discussing the paper and giving valuable criticism, the author is deeply indebted to Profs J. Duffy and L. B. Freund of the faculty of Mechanics of Solids and Structures, Brown University, for their guidance and support in the preparation of this report. Thanks are due also to Profs A. C. Pipkin and Visiting Assistant Prof G. Dassios of the faculty of Applied Mathematics, Brown University, for their kind advice on specific points. Lastly, the author would like to thank the office of Naval Research, Contract N00014-78-C-0051, and the Materials Research Laboratory, Brown University, for their support.

REFERENCES

[1] P. Manogg, *Anwendung der Schattenoptik zur Untersuchung des Zerreissvorganges von Platten* Dissertationsschrift an der Universität Freiburg (1964).
[2] P. S. Theocaris, Local yielding around a crack tip in plexiglass. *J. Appl. Mech.* **37**, 409–415 (1970).
[3] P. S. Theocaris, Reflected shadow method for the study of constrained zones in cracked plates. *Appl. Optics* **10**, 2240–2247 (1971).
[4] P. S. Theocaris and E. E. Gdoutos, An optical method for determining opening-mode and edge sliding-mode stress intensity factors. *J. Appl. Mech.* **39**, 91–97 (1972).
[5] P. S. Theocaris and E. E. Gdoutos, Surface topography by caustics. *Appl. Optics* **15**, 1629–1638 (1976).
[6] P. S. Theocaris, Dynamic propagation and arrest measurements by the method of caustics on overlapping skew-parallel cracks. *Int. J. Solids Structures* **14**, 639–653, (1978).
[7] D. D. Raftopoulos, D. Karapanos and P. S. Theocaris, Static and dynamic mechanical and optical behavior of high polymers. *J. Phys. D (Appl. Phys.)* **9**, 869–877 (1976).
[8] F. Katsamanis, D. Raftopoulos and P. S. Theocaris, Static and dynamic stress intensity factors by the Method of Transmitted Caustics. *J. Engin. Mat. and Tech.* **99**, 105–109 (1977).
[9] J. F. Kalthoff, J. Beinert and S. Winkler, Influence of dynamic effects on crack arrest. *Institut für Festkörpermechanik, Tech. Rep.* August (1978).
[10] J. F. Kalthoff, J. Beinert, S. Winkler and J. Blauel, On the Determination of the Crack Arrest-Toughness, *4th Int. Conf. Fracture*, Waterloo, Canada, 3, 751 ff (1977).
[11] P. S. Theocaris and F. Katsamanis, Response of cracks to impact by caustics. *Engng Fracture Mech.* **10**, 197–210 (1978).
[12] L. B. Freund and R. J. Clifton, On the uniqueness of plane elastodynamic solutions for running cracks. *J. Elasticity* **4**, (4) 293–299 (1974).
[13] L. B. Freund, Dynamic crack propagation. *Mech. of Fracture* AMD 19, 105–134 (1976).
[14] L. B. Freund, The analysis of elastodynamic crack tip stress fields. *Mech. Today* **3**, 55–91 (1976).
[15] H. Bergkvist, The motion of a brittle crack. *J. Mech. Phys. Solids* **21**, 299–339 (1973).
[16] T. L. Paxson and R. A. Lucas, *An Experimental Investigation of the Velocity Characteristics of a Fixed Boundary Fracture Model, Dynamic Crack Propagation* (Edited by G. C. Sih), Noordhoff, Leyden, p. 415 (1973).

[17] H. Schardin, Velocity effects in fracture, *Fracture*, p. 297. (Edited by B. L. Averback *et al.*) Wiley, New York (1959).
[18] E. N. Dulaney and W. F. Brace, Velocity Behaviour of a Growing Crack. *J. Appl. Phys.* **31**, (12) 2233–2236 (1960).
[19] B. Cotterell, Velocity effects in fracture propagation. *Appl. Math. Res.* **4**, 227–232 (1965).
[20] L. Dahlberg, Experimental studies of crack propagation in polymers. *R. Inst. Tech.*, Stockholm (1972).
[21] D. H. Davies and S. C. Hunter, The dynamic compression testing of solids by the method of the split Hopkinson pressure bar. *J. Mech. Phys. Solids* **11**, 155–179 (1963).
[22] F. Katsamanis, D. Raftopoulos, P. S. Theocaris, The dependence of crack velocity on the critical stress in fracture. *Exp. Mech.* **17**, (4) 128–132 (1977).
[23] L. B. Freund, Private Communication (1979).

(*Received* 23 *July* 1979; *received for publication* 23 *August* 1979)

APPENDIX

A1. (*i*) *Mixed mode propagating cracks*

As we have seen in Section 1 the deviation from parallelism of a reflected light ray at a distance z_0 from the middle surface of the specimen, can be expressed as:

$$W = C\,\mathrm{grad}_{x,y}(\sigma_{xx} + \sigma_{yy}) \qquad \text{where} \quad C = \frac{\mathrm{d}yz_0}{E}.$$

When the crack tip deformation is a combination of the plane Modes I and II, the expressions for σ_{xx} and σ_{yy} developed by Freund [23] following the procedure of [12] are given by:

$$\sigma_{xx} = \frac{K_{Id}(t)}{\sqrt{2\pi}} B_I(V)\left[(1 + 2\alpha_l^2 - \alpha_s^2)\frac{\cos(\theta_l/2)}{r_l^{1/2}} - \frac{4\alpha_s\alpha_l\cos(\theta_s/2)}{(1+\alpha_s^2)r_s^{1/2}}\right]$$

$$- \frac{K_{IId}(t)}{\sqrt{2\pi}} B_{II}(V)\left[(1 + 2\alpha^2 - \alpha_s^2)\frac{\sin(\theta_l/2)}{r_l^{1/2}} - (1+\alpha_s^2)\frac{\sin(\theta_s/2)}{r_s^{1/2}}\right] \tag{A1.1}$$

and

$$\sigma_{yy} = \frac{K_{Id}(t)}{\sqrt{2\pi}} B_I(V)\left[-(1+\alpha_s^2)\frac{\cos(\theta_l/2)}{r_l^{1/2}} + \frac{4\alpha_l\alpha_s}{(1+\alpha_s^2)}\cdot\frac{\cos(\theta_s/2)}{r_s^{1/2}}\right]$$

$$- \frac{K_{IId}(t)}{\sqrt{2\pi}} B_{II}(V)\left[-\frac{\sin(\theta_l/2)}{r_l^{1/2}}(1+\alpha_s^2) + \frac{\sin(\theta_s/2)}{r_s^{1/2}}(1+\alpha_s^2)\right] \tag{A1.2}$$

where

$$B_I(V) = \frac{(1+\alpha_s^2)}{[4\alpha_l\alpha_s - (1+\alpha_s^2)^2]}$$

and

$$B_{II}(V) = \frac{2\alpha_s}{[4\alpha_l\alpha_s - (1+\alpha_s^2)^2]}.$$

The above expressions were derived under the assumption of elastic fracture behaviour with V representing the instantaneous crack tip speed for nonuniform rates of crack growth. Adding (A1.1) and (A1.2) we obtain:

$$\sigma_{xx} + \sigma_{yy} = (\alpha_l^2 - \alpha_s^2)K_{Id}(t)B_I\sqrt{\frac{2}{\pi r_l}}\cos(\theta_l/2)$$

$$-(\alpha_l^2 - \alpha_s^2)K_{IId}(t)B_{II}\sqrt{\frac{2}{\pi r_l}}\sin(\theta_l/2).$$

Setting now

$$B_I K_{Id}(t)(\alpha_l^2 - \alpha_s^2) = K_I' \qquad \text{and} \qquad B_{II}K_{IId}(t)(\alpha_l^2 - \alpha_s^2) = K_{II}' \tag{A1.3}$$

we have:

$$\sigma_{xx} + \sigma_{yy} = K_I'\sqrt{\frac{2}{\pi r_l}}\cos(\theta_l/2) - K_{II}'\sqrt{\frac{2}{\pi r_l}}\sin(\theta_l/2). \tag{A1.4}$$

It is worth observing that the above expression describing the first stress invariant near the tip of the propagating crack is of the same functional form as the equivalent static one.

(ii) *The equations of the mapping.* The coordinates of a point $P'(X, Y)$ on the screen which is the image of a point $P(x, y)$ of the specimen are given by eqns (2.5) with respect to the first stress invariant, as follows:

$$\left.\begin{aligned} X &= x + C\frac{\partial}{\partial x_l}[(\sigma_{xx} + \sigma_{yy})(x_l, y_l)] \\ Y &= y + \alpha_l C\frac{\partial}{\partial y_l}[(\sigma_{xx} + \sigma_{yy})(x_l, y_l)] \end{aligned}\right\}$$

Substituting expression (A1.4) in the above equations, and using the fact that $x = r_l \cos\theta_l$ and $y_l = \dfrac{r_l \sin\theta_l}{\alpha_l}$, we get:

$$\left.\begin{aligned} X &= r_l\cos\theta_l + \lambda r_l^{-3/2}\left(K_I'\cos\frac{3\theta_l}{2} - K_{II}'\sin\frac{3\theta_l}{2}\right) \\ Y &= \frac{1}{\alpha_l}\left(r_l\sin\theta_l + \alpha_l^2\lambda r_l^{-3/2}\left(K_I'\sin\frac{3\theta_l}{2} + K_{II}'\cos\frac{3\theta_l}{2}\right)\right) \end{aligned}\right\} \tag{A1.5}$$

where $\lambda = \dfrac{C}{(2\pi)^{1/2}}$ and $0 < \theta_l < 4\pi$.

Equations (A1.5) are the governing equations for the mapping of a generic point $P(x, y)$ of the specimen on to a point $P'(X, Y)$ of the screen.

(iii) *The equations of the initial curve.* The condition for the existence of a caustic curve is the vanishing of the Jacobian of the transformation (A1.5).

Performing a calculation similar to the one described in Section 2(ii) for the case of an opening mode crack we get a curve with respect to the (r_l, θ_l) parameters which is the image of the "initial curve" in the (r_l, θ_l) plane. This curve is obtained by setting $J = \dfrac{\partial(X, Y)}{\partial(x, y)} = \alpha_l\dfrac{\partial(X, Y)}{\partial(x_l y_l)} = 0$. and in polar form it is given as:

$$r_l^5 - \tfrac{9}{4}\lambda^2\alpha_l^2(K_I'^2 + K_{II}'^2) + \tfrac{3}{2}\lambda r_l^{5/2}(\alpha_l^2 - 1)\left[K_I'\cos\frac{5\theta_l}{2} - K_{II}'\sin\frac{5\theta_l}{2}\right] = 0. \tag{A1.6}$$

The above equations can be expressed in the following form:

$$r^5 - \tfrac{9}{4}\lambda^2\alpha_l^2(K_I'^2 + K_{II}'^2) + \tfrac{3}{2}\lambda r_l^{5/2}(\alpha_l^2 - 1)(K_I'^2 + K_{II}'^2)^{1/2}\cos\tfrac{5}{2}(\theta_l + \chi) = 0 \tag{A1.7}$$

where

$$\chi = \tfrac{5}{2}\tan^{-1}\frac{K_{II}'}{K_I'} = \tfrac{5}{2}\tan^{-1}\left[\frac{K_{IId}(t)}{K_{Id}(t)}\cdot\frac{2\alpha_s}{(1 + \alpha_s^2)}\right]$$

for $K_{IId}(t) = 0$ the above reduces to eqn (2.8) in Section 2(ii). The exact equations of the caustic envelope are therefore given by:

$$\left.\begin{aligned} X &= r_l\cos\theta_l + \lambda r_l^{-3/2}\left(K_I'\cos\frac{3\theta_l}{2} - K_{II}'\sin\frac{3\theta_l}{2}\right) \\ Y &= \frac{1}{\alpha_l}(r_l\sin\theta_l + \alpha_l^2\lambda r_l^{-3/2}\left(K_I'\sin\frac{3\theta_l}{2} + K_{II}'\cos\frac{3\theta_l}{2}\right) \end{aligned}\right\} \tag{A1.8}$$

under the constraint:

$$r_l^5 - \tfrac{9}{4}\lambda^2\alpha_l^2(K_I'^2 + K_{II}'^2) + \tfrac{3}{2}\lambda r_l^{5/2}(\alpha_l^2 - 1)\left[K_I'\cos\frac{5\theta_l}{2} - K_{II}'\sin\frac{5\theta_l}{2}\right] = 0$$

using the same approximation scheme as the one adopted in Section 3, we will try to find a set of circles each of which constitutes the best fit to (A1.6) for each value of α_l. To do so the area of a random member of the family of images (A1.5) is calculated with respect to r_l. The expression is subsequently differentiated, giving the critical radius $r_l = \rho_0$ corresponding to the minimum area image. The area of a member is given by:

$$E = \frac{1}{2}\int_0^{4\pi}(XY_{\theta_l}' - YX_{\theta_l}')\,d\theta_l.$$

Using expressions (A1.5) we can show that

$$E = \frac{1}{2}\frac{4\pi}{\alpha_l}[r_l^2 - \tfrac{3}{2}\lambda^2(K_I'^2 + K_{II}'^2)\alpha_l r_l^{-3}].$$

The conditions for the minimum gives

$$\left.\frac{\partial E}{\partial r_l}\right|_{r_l=\rho_0} = 0 \Rightarrow \rho_0 = [\tfrac{3}{2}\lambda\sqrt{K_I'^2 + K_{II}'^2}\,\alpha_l]^{2/5} \tag{A1.9}$$

Thus $\rho_0 = [\frac{3}{2}\lambda\alpha_l\sqrt{K_I'^2 + K_{II}'^2}\,]^{2/5}$ corresponds to the closest circle approximation to the curve represented by equation (A1.6). One can see that the two curves touch at a total of five points. The coordinates of these five points in the (r_l, θ_l) plane depend on the value of the ratio

$$\xi = \frac{K_{II}'}{K_I'} = \frac{2\alpha_s}{(1+\alpha_s^2)} \cdot \frac{K_{IId}(t)}{K_{Id}(t)}$$

and will be given by substituting

$$r_l = \rho_0 = [\tfrac{3}{2}\lambda\alpha_l\sqrt{K_I'^2 + K_{II}'^2}\,]^{2/5}$$

in (A1.6). The substitution gives:

$$\cot\left(\frac{5\theta_l}{2}\right) = \frac{K_{II}'}{K_I'} = \xi. \tag{A1.10}$$

For the special case of $K_{IId}(t) = 0 \Rightarrow K_{II}' = 0$, we have seen in Section 3, that θ_l takes the values of $\pi/5$, $3\pi/4$, π, $7\pi/5$, $9\pi/5$ which are independent of the velocity of the crack.

For non-zero $K_{IId}(t)$, the coordinates of the five common points will be functions of both $K_{IId}(t)$ and α_s as shown in (A1.10).

Figure 7 shows the effect of a finite $K_{IId}(t)$. The axis of symmetry of the curve described by (A1.6) (dotted line) in the (x_l, y_l) plane, will be rotated through an angle $\chi = \frac{2}{5}\tan^{-1}\left[\frac{K_{IId}(t)}{K_{Id}(t)} \cdot \frac{2\alpha_s}{(1+\alpha^2)}\right]$ with respect to the x_l axis, which coincides with the tangent to the crack tip.

(iv) *Best approximation of the initial curve in the* (x, y) *plane.* As shown above, the equation of the best circle approximation to the curve (A1.6) (image of the initial curve in the (x_i, y_i) plane) is given by:

$$x_l^2 + y_l^2 = [\tfrac{3}{2}\alpha_l\lambda\sqrt{K_I'^2 + K_{II}'^2}\,]^{4/5}.$$

In the (x, y) specimen plane, the corresponding points (r, θ) lie on the ellipse

$$x^2 + \alpha_l^2 y^2 = [\tfrac{3}{2}\alpha_l\lambda\sqrt{K_I'^2 + K_{II}'^2}\,]^{4/5} = \rho_0^2 \tag{A1.11}$$

which can be expressed as:

$$x^2 + \alpha_l^2 y^2 = \left[\frac{3}{2}\left(\frac{(1+\alpha_s^2)(\alpha_l^2 - \alpha_s^2)}{4\alpha_l\alpha_s - (1+\alpha_s^2)^2}\right)\alpha_l \frac{dvz_0}{E(2\pi)^{1/2}} K_{Id}(t)\right]^{4/5} (1+\xi^2)^{2/5} = \rho_0^2.$$

For $K_{IId}(t) = 0 \Rightarrow \xi = 0$, the above reduces to eqn (4.1) obtained for a mode I crack.

(v) *The behavior of the initial curve as* $V \to 0$. Letting $V \to 0$, both $\alpha_l, \alpha_s \to 1$ and $K_I' \to K_I$, $K_{II}' \to K_{II}$. Equation (A1.11) therefore reduces to

$$x^2 + y^2 = [\tfrac{3}{2}\lambda\sqrt{K_I^2 + K_{II}^2}\,]^{4/5} = \rho_{st}^2$$

which is the known equation of the initial curve obtained using the stress field of a stationary crack [4].

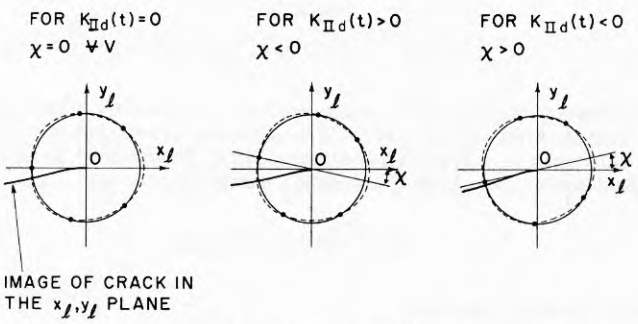

Fig. 7. The effect of a finite $K_{IId}(t)$; Dotted line: the image of the initial curve in the (x_l, y_l) plane; Solid line: its best circle approximation.

A2. (i) *The approximate equations of the caustic curve*
After the approximation is made, eqn (A1.8) become:

$$\left.\begin{aligned} X &= r_l \cos\theta_l + \lambda r_l^{-3/2}\left(K_I' \cos\frac{3\theta_l}{2} - K_{II}' \sin\frac{3\theta_l}{2}\right) \\ Y &= \frac{1}{\alpha_l}(r_l \sin\theta_l + \alpha_l \lambda r_l^{-3/2}\left(K_I' \sin\frac{3\theta_l}{2} + K_{II}' \cos\frac{3\theta_l}{2}\right) \end{aligned}\right\} \tag{A2.1}$$

where

$$r_l = [\tfrac{3}{2}\lambda\alpha_l\sqrt{K_I'^2 + K_{II}'^2}\,]^{2/5} = \rho_0.$$

Equation (A2.1) can be expressed as follows:

$$\left.\begin{aligned} X &= \rho_0\left[\cos\theta_l + \frac{2}{3}\frac{1}{(1+\xi^2)^{1/2}}\cdot\frac{1}{\alpha_l}\cos\frac{3\theta_l}{2} - \frac{2}{3}\frac{\xi}{(1+\xi^2)^{1/2}}\frac{1}{\alpha_l}\cdot\sin\frac{3\theta_l}{2}\right] \\ Y &= \frac{\rho_0}{\alpha_l}\left[\cos\theta_l + \frac{2}{3}\frac{1}{(1+\xi^2)^{1/2}}\alpha_l\sin\frac{3\theta_l}{2} + \frac{2}{3}\frac{\xi}{(1+\xi^2)^{1/2}}\alpha_l\cos\frac{3\theta_l}{2}\right] \end{aligned}\right\}$$

where

$$\xi = \frac{K_{II}'}{K_I'}.$$

Setting now $\xi = \tan\phi'$ the equations of the caustic curve can be finally expressed as:

$$\left.\begin{aligned} X &= \rho_0\left[\cos\theta_l + \tfrac{2}{3}\alpha_l^{-1}\cos\left(\frac{3\theta_l}{2} + \phi'\right)\right] \\ Y &= \frac{\rho_0}{\alpha_l}\left[\sin\theta_l + \tfrac{2}{3}\alpha_l\sin\left(\frac{3\theta_l}{2} + \phi'\right)\right] \end{aligned}\right\} \tag{A2.2}$$

where

$$\phi' = \tan^{-1}\frac{K_{II}'}{K_I'} = \tan^{-1}\left[\frac{2\alpha_s}{1+\alpha_s^2}\frac{K_{IId}(t)}{K_{Id}(t)}\right].$$

The above equations are the parametric equations of the caustic curve for a case of a mixed mode propagating crack.

(ii) *Behavior as* $V \to 0$. As $V \to 0$ and $\alpha_{l,s} \to 1$, $\omega' \to \tan^{-1}\left(\frac{K_{II}}{K_I}\right) = \phi$, $\theta_l \to \theta$, $\rho_0 \to \rho_{st}$ and the above equations become:

$$\left.\begin{aligned} X &= \rho_{st}\left[\cos\theta + \frac{2}{3}\cos\left(\frac{3\theta}{2} + \phi\right)\right] \\ Y &= \rho_{st}\left[\sin\theta + \frac{2}{3}\sin\left(\frac{3\theta}{2} + \phi\right)\right] \end{aligned}\right\} \tag{A2.3}$$

which, as expected, are the equations of the caustic curve for the case of a stationary mixed mode crack [4].